Radiological Assessment of the Shoulder

10

Üstün Aydıngöz

10.1 Introduction

Radiology has several roles in the assessment and management of shoulder disorders. First and foremost, it gives important clues about the underlying conditions or the exact cause of shoulder pain, which, frequently along with restricted range of motion, is the most common symptom of this joint. Second, radiological imaging provides guidance in selecting treatment choices as well as determining the type and extent of surgery to be performed in problems such as rotator cuff tears and bony Bankart lesions. Third, imaging is an important tool in the assessment of the glenohumeral and/or acromioclavicular joints following treatment or surgery. Last but not the least, radiology can also be used directly in the treatment of some conditions (e.g., ultrasonography-guided lavage of calcific deposits in calcific tendinitis) and for the intra-articular injection of anesthetics and/or corticosteroids.

10.2 Radiological Modalities and Techniques of Shoulder Imaging

Radiological armamentarium available for the shoulder joint includes radiography, arthrography, ultrasonography, computed tomography, and magnetic resonance imaging. Each of these modalities has special roles and techniques employed in the assessment of shoulder conditions ranging from traumatic to degenerative and inflammatory to neoplastic. Selection of the imaging modality to be used and determination of the technical aspects of the radiological examination depend on the nature of the underlying condition and/or presenting symptom of the patient. It is therefore of crucial importance to provide the radiologist with correct, relevant, and sufficient clinical information at the time of requesting these procedures. Sometimes, the radiologist might change or fine-tune the modality or technique in view of the patient characteristics or presumptive diagnosis.

10.2.1 Radiography

Similar to its use elsewhere in the musculoskeletal system, radiography is usually the first-line imaging tool for the shoulder. Overall, a set of internal and external rotation anteroposterior (AP) views and a scapular Y view is a commonly

Ü. Aydıngöz (✉)
Department of Radiology, Hacettepe University School of Medicine, Ankara, Turkey
e-mail: uaydingo@hacettepe.edu.tr

G. Huri et al. (eds.), *Fundamentals of the Shoulder*, https://doi.org/10.1007/978-3-030-94702-6_10

used combination [1]. Internal and external rotation AP views profile the middle and superior facets of the greater humeral tubercle, and thereby the infraspinatus and supraspinatus tendon insertions, respectively. Scapular Y view shows the glenoid joint surface *en face,* displaying the relationship of the humeral head with respect to the glenoid fossa. Axillary view, which also shows this relationship and profiles the glenohumeral joint, is not easy to obtain in the posttraumatic painful setting. If the arm cannot be sufficiently abducted for the classic axillary view, modifications to the axillary view, including the Velpeau view, can be made. Another variant of AP views is the Grashey view, which profiles the glenohumeral joint and is obtained while the patients rotate their body 45° with respect to the X-ray detector by distancing their contralateral shoulder away from the detector surface. I recommend replacing external rotation AP view with Grashey view in routine work-up of patients with shoulder pain as the latter profiles not only the glenohumeral joint but also the supraspinatus tendon insertion, and displays the critical shoulder angle (CSA), which was shown by multiple studies to be a relevant predictor for the development of either osteoarthritis or rotator cuff tears (Fig. 10.1) [2] (see Sect. 10.3.1).

Fig. 10.1 Radiographic Grashey view is a 45° oblique anteroposterior projection that profiles the glenohumeral joint. Critical shoulder angle (CSA) forms between a line through the superior and inferior margins of the glenoid cavity and a line through the inferior glenoid margin and lateral acromial margin. Some studies suggest that a CSA >35° correlates with rotator cuff tears and a CSA <30° correlates with osteoarthritis of the glenohumeral joint [2]

10.2.2 Arthrography

X-ray arthrography has become practically obsolete in musculoskeletal imaging. However, imaging guidance for intraarticular or parafascial/peritendinous/intrabursal therapeutic injections entails the use of either X-rays or ultrasonography. For the wrist, it is also important to follow during arthroscopic fluoroscopy the path of the injectate through joint compartments during stress maneuvers. For the shoulder joint, however, MR- and CT-arthrography has essentially replaced conventional X-ray arthrography.

10.2.3 Ultrasonography (US)

Ultrasonography is widely used in the assessment of rotator cuff tendons and long head of the biceps tendon (LHBT). An experienced operator is essential for the best use of US in the shoulder. Awareness of the imaging and positioning pitfalls, use of an appropriate transducer and rotatable chairs for the examiner and the patient, employment of specific positions of the patient's arm and forearm for different structures, and examination of the contralateral side as needed are among the key points in shoulder US. Major downsides of shoulder US are its limited ability to show intraarticular structures such as the glenoid labrum, the glenohumeral ligaments and the joint cartilage, and its inability to display bone marrow.

10.2.4 Computed Tomography (CT)

Computed tomography, which provides detailed information about the bony structures of the shoulder in a few minutes, is mostly used in the shoulder joint to characterize and classify acute occult or complex fractures, and to identify a bony Bankart (or reverse Bankart) lesion as well as to assess the glenoid bony stock [3].

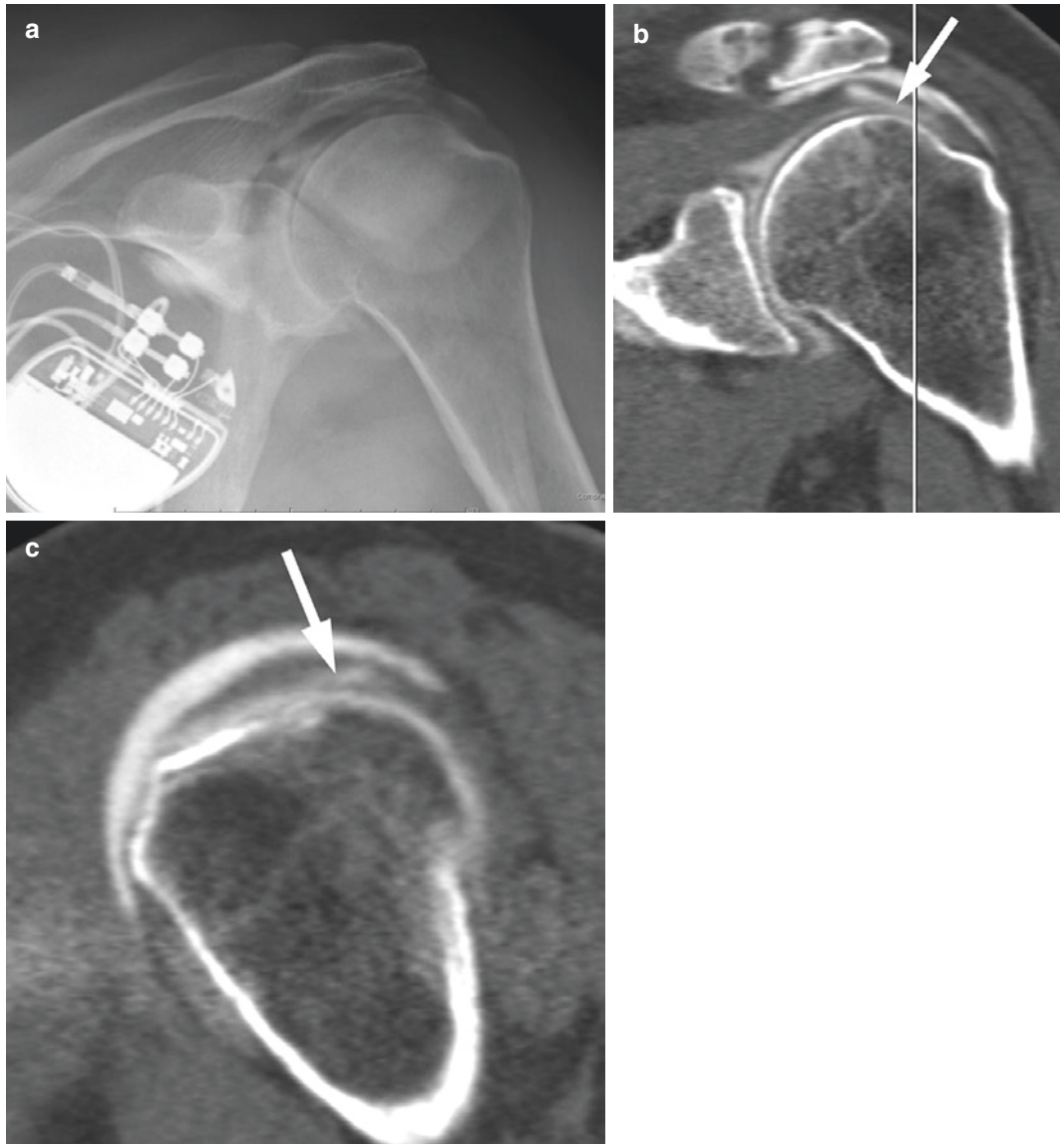

Fig. 10.2 CT-arthrography in a 59-year-old man, who could not undergo an MRI examination because of a cardiac defibrillator (**a**, fluoroscopy image obtained during intraarticular injection). Coronal oblique (**b**) and sagittal oblique (**c**) reformatted CT-arthrography images show a delamination tear at the supraspinatus tendon (*arrows*) (perpendicular line on **b** refers to the section on **c**)

The latter is facilitated by the possibility of excluding the humeral head from three-dimensional CT images [1]. When radiography is inconclusive for the assessment of shoulder arthroplasty complications, CT with metal artifact reduction software can show conditions such as loosening, scapular notching, and heterotopic ossification [4].

10.2.4.1 CT-Arthrography

After MR-arthrography began to be extensively used in the early years of this century, CT arthrography gained popularity, following its initial use in patients with MR-incompatible devices and claustrophobia (Fig. 10.2). CT arthrography might indeed be performed as a salvage procedure when what started as an MR-arthrography

procedure needs to be modified due to unanticipated claustrophobia or significant patient motion. In fact, cartilage lesions in the glenohumeral joint are detected on CT arthrography even better than on direct MR-arthrography [5]. CT-arthrography is also accurate in the detection of full-thickness and articular surface partial tears of the supraspinatus and infraspinatus, shows similar sensitivities and specificities with 3 T MR-arthrography in the assessment of lesions of the proximal LHBT, effectively detects superior labrum anterior-to-posterior (SLAP) lesions, and distinguishes between normal variants affecting the anterosuperior labrum and labral-bicipital complex [6].

10.2.5 Magnetic Resonance Imaging (MRI)

Magnetic resonance imaging is by far the most common cross-sectional imaging method used for the evaluation of shoulder joint. It superbly depicts all structures of the shoulder region relevant to the practice of clinicians, be it an orthopedic surgeon, a rheumatologist, or a physical therapy and rehabilitation expert. Its ability to exquisitely show osseous structures (in conditions like bone contusions, edema-like changes, and focal or infiltrative lesions) as well as soft tissues such as tendons, capsulolabral, and ligamentous structures makes MRI an excellent imaging tool for the assessment of the musculoskeletal system in general and the shoulder joint in particular. A novel imaging technique, called zero echo-time (ZTE) MRI, allows obtaining radiograph- or CT-like images during an MRI examination, making it easier in some cases to identify bony Bankart lesions and assess the glenoid track as well as bone stock [7, 8].

Many caveats related to MRI involve variant anatomy (see Sects. 10.3.1 and 10.4.1), imaging pitfalls [9, 10], and the possibility that some shoulder conditions might be encountered in asymptomatic persons (see Sect. 10.3.1). In other words, what appears to be a positive finding on MRI is not necessarily pathological or clinically significant.

The best use of MRI in the shoulder joint necessitates the use of a dedicated surface coil, optimal positioning of the arm, and forearm (usually lying alongside the patient's body with the palm of the hand facing either the patient's body or the ceiling—and not the examination table) with liberal padding to ensure avoidance of motion artifacts, and a tailored examination with imaging planes that best depict normal structures and their pathological conditions. Internal rotation of the shoulder during MRI results in anterior capsulolabral and ligamentous redundancy and can conceal tears at this region. Adding a sequence obtained in ABduction and External Rotation (ABER) would tension this region during MR-arthrography of the shoulder, which already helps overcome such redundancy with intraarticular contrast distention of the glenohumeral joint (see Sect. 10.2.5.1).

10.2.5.1 MR-Arthrography

MR-arthrography can be performed in two ways: indirect or direct. Indirect MR-arthrography employs the use of an intravenously administered contrast material, which diffuses into the glenohumeral joint in a few minutes during which the patients move their shoulder joint to facilitate the diffusion; magnetic resonance imaging then follows. Although it entails no need for the set-up of a fluoroscopy- or US-guided injection into the glenohumeral joint, indirect MR-arthrography suffers from the lack of distention of the joint in addition to the contrast enhancement of surrounding structures, which might mask some of the conditions investigated. Therefore, direct MR-arthrography, in which an injectate usually containing a gadolinium-based contrast agent is injected into the shoulder joint under imaging guidance, is much more commonly used.

Direct MR-arthrography is the best imaging method for the overall assessment of shoulder joint including the rotator cuff tendons, capsulolabral and ligamentous structures, LHBT, and articular cartilage. Imaging sequences built into direct MR-arthrography also allow visualization of the muscles and bone marrow. Although recent studies have demonstrated gadolinium

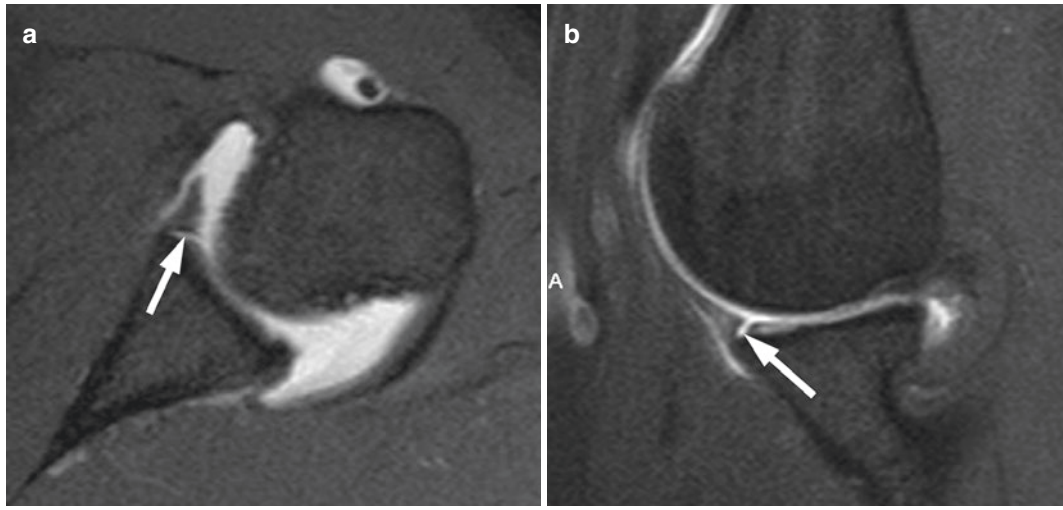

Fig. 10.3 Perthes lesion (*arrows*) denoting a non-displaced tear of the anteroinferior labrum on a transverse fat-saturated T1-weighted MR-arthrography image (**a**) in a 29-year-old man is better depicted on the oblique fat-saturated T1-weighted image (**b**) obtained at the abduction and external rotation (ABER) position

deposition in the brain in patients with normal renal function following intravenous gadolinium-based contrast agent administration, investigators of a recent study found no MRI evidence of intracranial gadolinium deposition following MR-arthrography [11].

From a technical standpoint, MR-arthrography of the shoulder can be made using an anterior or preferably a posterior approach. Anterior approach runs the risk of contaminating the subacromial-subdeltoid bursa by way of inadvertently injecting into the subcoracoid bursa (these two bursae are connected in some patients): The subacromial-subdeltoid bursa could have been otherwise filled by a full-thickness supraspinatus and/or infraspinatus tendon tear and anterior injection might compromise the diagnosis of such a tear, especially when it is small.

Addition of the ABER sequence to MR-arthrography of the shoulder helps depict better some glenohumeral joint structures and surrounding tissues under a position relevant to several pathologic conditions. The abduction and external rotation position during this sequence tensions the anteroinferior glenohumeral ligament and labrum and releases tension on the supraspinatus and infraspinatus relative to the normal coronal view obtained with the arm in adduction. Among the lesions better shown in this position are subtle partial-thickness articular sided tears of the supraspinatus and infraspinatus tendons (Fig. 10.3), subtle tears of the anteroinferior portion of the glenoid labrum (such as the Perthes lesion) and anterior band of the inferior glenohumeral band [12].

10.3 Imaging in Rotator Cuff Abnormalities

Rotator cuff muscles and tendons are best displayed on MRI or MR-arthrography. Radiographs are a useful adjunct in this regard and should be the first-line imaging tool. Ultrasonography is also being increasingly used in the assessment—and sometimes during treatment—of rotator cuff abnormalities.

10.3.1 Rotator Cuff Tendonosis and Tendon Tears

Rotator cuff disorders are a major source of shoulder pain. Rotator cuff tendinopathy is an

umbrella term that encompasses tendon tears and tendonosis (the latter covers both tendon inflammation and degeneration). Tendonosis on MRI refers to the mild signal increase within a tendon which does not amount to fluid intensity, which usually means a tear. Although US has been validated for the assessment of rotator cuff tears with reported sensitivities and specificities that rival that of conventional MRI, it is with MRI that a more comprehensive evaluation of the shoulder, including more accurate appraisal of articular cartilage and labroligamentous structures as well as depiction of the bones, is possible [13]. A partial-thickness tear involves either the substance or the articular or, less commonly, bursal side of a rotator cuff tendon. Considering an expected thickness of 10–12 mm for a tendon, small and medium tears are 3 mm deep and 3–6 mm deep, respectively, both involving less than 50% of tendon thickness [13]. Large partial-thickness tears, still non-communicating as the small and medium tears, involve greater than 50% of tendon thickness. Delaminating tears are longitudinally oriented and involve the tendon substance, sometimes reaching the articular or bursal surface at one (commonly the distal) end (Fig. 10.4). Easily identified on MRI, such tears are difficult to visualize at arthroscopy. Although full-thickness tears by definition communicate between the articular and bursal sides of the cuff, a small percentage of them fail to show the characteristic fluid or gadolinium-based contrast filled "communicating gap" appearance on MRI or MR-arthrography, respectively. Instead, there might be a heterogeneous T2 signal, likely due to inflammation with subsequent granulation tissue formation within the region of tear, volume averaging pitfall of small tears, or coaptation of torn tendon edges [13]. The best practice on reporting MRI is to describe the location and three-dimensional extent of all rotator cuff tendon tears (partial or full thickness) (Fig. 10.5). As important full-thickness rotator cuff tear descriptors on MRI, tear size, degree of tendon retraction, and degrees of atrophy and fatty infiltration of muscles help guide surgical management [13]. Intramuscular "sentinel cysts" and humeral head cysts at or near the footprints of rotator cuff tendons can help in the MRI diagnosis or suggestion of rotator cuff tears in cases with equivocal findings. Anterior humeral cysts at the supraspinatus and subscapularis tendon insertions show a high correlation with rotator cuff disorders, whereas cysts at the infraspinatus tendon insertion and posterolateral "bare area" at the anatomic neck have little such correlation, are asymptomatic and likely related to vascular intrusions [14].

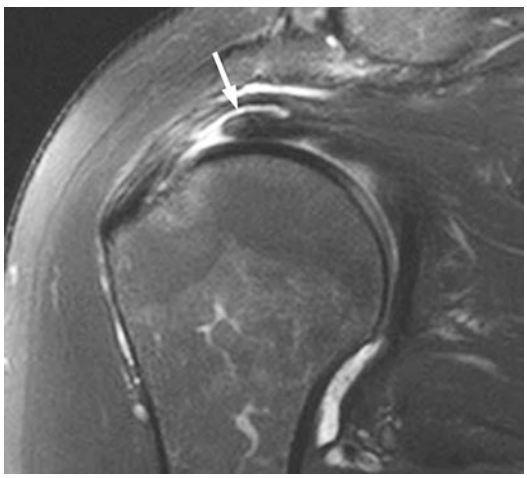

Fig. 10.4 Coronal oblique fat-saturated T2-weighted MR image shows a Partial thickness Articular-sided tear with INTratendinous extension (i.e., delamination, *arrow;* the so-called PAINT lesion) in the background of infraspinatus tendonosis

MRI findings of rotator cuff tendonosis and tears do not necessarily correspond to shoulder problems. In other words, asymptomatic persons can have rotator cuff tendonosis and tears on MRI. Up to 46% of entire population and nearly 40% of persons over 60 years of age may have rotator cuff tears [15]. Up to 40% of elite overhead athletes have partial or full thickness rotator cuff tears on MRI with no reported problems [16].

Subscapularis tendon evaluation on routine MRI is challenging. Although MR-arthrography is quite sensitive and specific for subscapularis tears, routine MRI has a lower sensitivity [13]. A four-step approach to subscapularis evaluation may improve the sensitivity of MRI: Start with transverse fluid-sensitive images, evaluate LHBT for evidence of subluxation, assess subscapularis fatty infiltration or atrophy on T1-weighted

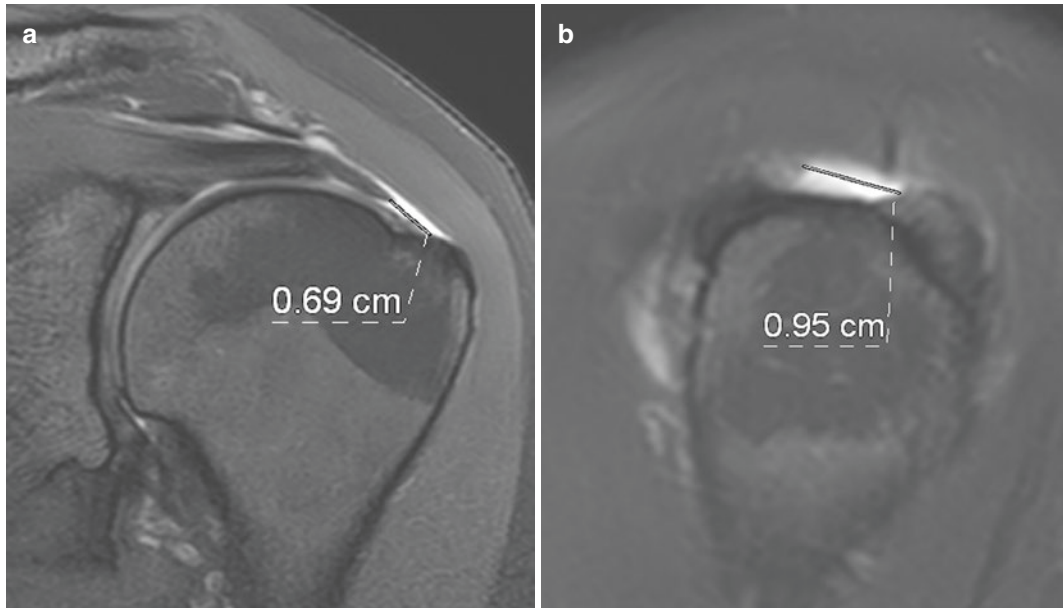

Fig. 10.5 Coronal oblique (**a**) and sagittal oblique (**b**) fat-saturated T2-weighted MR images show a full-thickness tear of the supraspinatus tendon with size measurements

images, and look for a tear on fluid-sensitive sagittal oblique images [17].

MRI plays an important role in identifying the "novel lesion" of the infraspinatus, which is an isolated atraumatic rupture of the interstitial infraspinatus (Fig. 10.6) [18]. Visualization of such tears is challenging at arthroscopy, they may progress to severe atrophy, and MRI guidance is essential in surgical intervention.

Assessment of the muscle stock associated with rotator cuff tears is an important contribution of radiological imaging. Goutallier et al.'s staging, which was described on CT and later modified by Fuchs et al. for MRI, and the tangent method on MRI are routinely used in the evaluation of rotator cuff muscle quality and quantity, respectively [19, 20].

Degenerative rotator cuff disease can manifest itself on radiographs with entheseal changes at the tendon insertions such as osteopenia, bony sclerosis, surface irregularity, and cyst formation [14]. Acromion morphology based on T1-weighted sagittal oblique MRI may be inferiorly flat, curved (most common), hooked (associated with increased incidence of impingement), or convex (upturned). Reporting on MRI of an os acromiale is important; when unreported and if unstable, this unfused ossification center, which normally appears at around 15 years of age and fuses by the age of 25 years [9], might compromise rotator cuff surgery. Critical shoulder angle (CSA) integrates two risk factors of rotator cuff tears by quantifying the extent of acromial coverage of the humerus and the inclination of the glenoid [2]. As a simple and highly reproducible parameter, CSA is a promising—yet controversial—tool for discriminating between rotator cuff tears and osteoarthritis (Fig. 10.1). Pre- and postoperative CSA measurements also appear to be useful for assessing the retear risk [2]. Unfortunately, routine MRI (without an isotropic 3D gradient echo or the recently introduced ZTE sequence) is not convenient for the measurement of CSA, which is readily displayed on an appropriately obtained radiographic Grashey view (see Sect. 10.2.1).

Postoperative evaluation of the shoulder for a retear is mostly made with MRI or, better, MR-arthrography. A 1.5 Tesla (T) system should be preferred over 3 T MRI equipment as artifacts created by surgical implants are more problem-

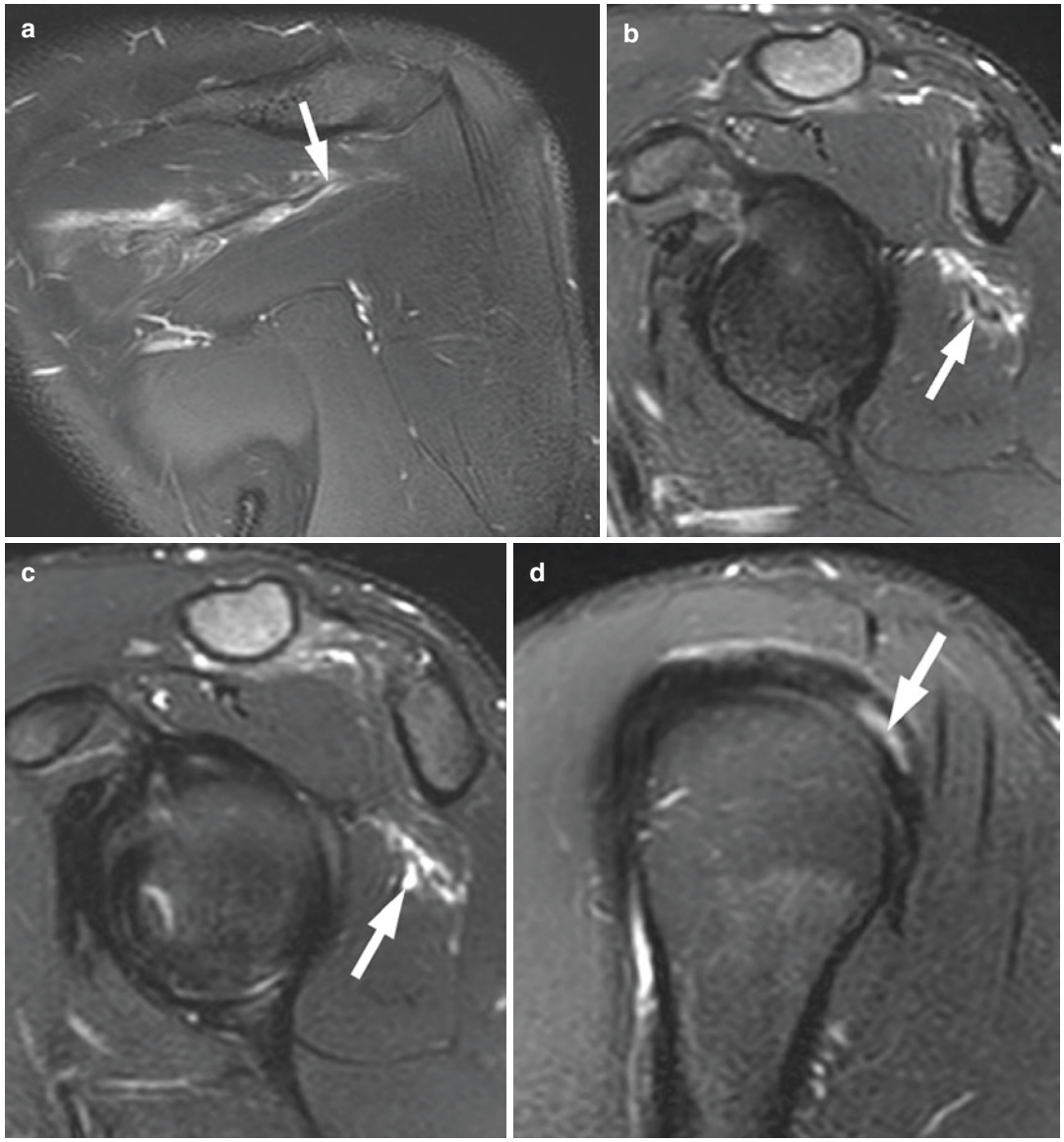

Fig. 10.6 Coronal oblique (**a**) and sagittal oblique (**b–d**) fat-saturated T2-weighted MR images show a retracted (*arrow,* **a**) delaminated intrasubstance (*arrows,* **c**, **d**) tear of the infraspinatus tendon (the "novel" lesion), associated with myotendinous junction edema (**a**, **b**) in a 24-year-old man who felt sudden pain during weightlifting. Such tears might not be seen on arthroscopy

atic on the latter. Metal artifact reduction sequences need to be employed. CT-arthrography or US may need to be substituted for MRI in the postoperative setting. Repair does not provide a "watertight" cuff and subacromial–subdeltoid bursal fluid, which might even communicate into this bursa from the glenohumeral joint during MR-arthrography, is not necessarily abnormal [21]. Repaired tendon can appear heterogeneous and thin on MRI (Fig. 10.7). Edema-like signal can be seen at the humeral head. Fluid-filled defect within the tendon suggests "retear."

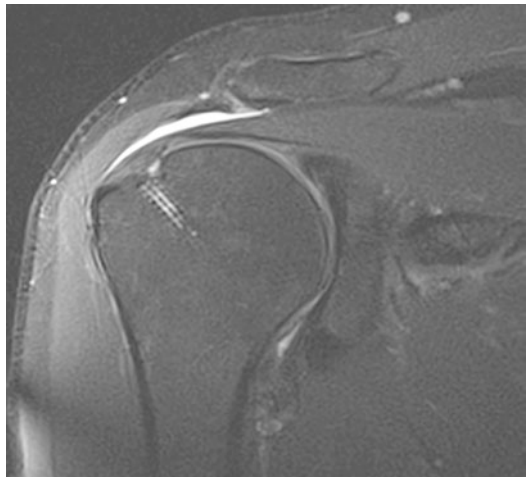

Fig. 10.7 Coronal oblique fat-saturated T2-weighted MR image shows a repaired supraspinatus tendon without retear. Repaired tendon can appear heterogeneous and thin on MRI

10.3.2 Rotator Cuff Tear Arthropathy

Massive tears of the rotator cuff can result in rotator cuff tear arthropathy, which has characteristic imaging findings on radiography and MRI. The acromiohumeral interval is narrowed (<7 mm) with superior migration of the humeral head, proximal humerus is "femoralized" because of the repetitive hitting of the greater tubercle to the acromion in the absence of a buffering rotator cuff, and "acetabularization" (rounding) of the coracoacromial arch occurs as an adaptation (Fig. 10.8) [22]. The resulting secondary osteoarthritis of the glenohumeral joint, with a more superiorly conspicuous joint cartilage loss, is usually different from primary shoulder osteoarthritis.

Although technically challenging to repair, massive rotator cuff tears are not necessarily irreparable. However, static superior migration of the humeral head, along with a narrowed or absent acromiohumeral interval and fatty infiltration affecting 50% or more of the rotator cuff muscles, is among the signs of irreparability and currently rotator cuff tear arthropathy is a major indication for reverse total shoulder arthroplasty [22].

With a massive rotator cuff tear, glenohumeral articular and subacromial-subdeltoid bursal fluid may gain access to the acromiohumeral (AC) joint through an eroded inferior AC joint capsule. This fluid can then traverse the AC joint to present as a cystic mass overlying the AC joint under the skin. This finding on MRI is called "the geyser sign" and suggests rotator cuff tear arthropathy.

10.3.3 Milwaukee Shoulder

The very rare unique combination of glenohumeral joint effusion with hydroxyapatite crystal deposition, rotator cuff tear(s), and rapidly destructive arthropathy is known as "Milwaukee shoulder" (Fig. 10.9). This condition is classically seen in the dominant hand side over 60 years of age and predominantly females. When bilateral, this condition is almost always more advanced on the dominant side. Although shoulder involvement is more common, the knees and the hips can also be affected [23, 24].

10.3.4 Adhesive Capsulitis (Frozen Shoulder)

Although adhesive capsulitis is typically a clinical diagnosis made on the basis of patient's history and physical examination, rotator cuff abnormalities and osteoarthritis can sometimes cause similar symptoms and signs, therefore necessitating imaging to rule it in or out. On MRI, findings suggestive of adhesive capsulitis include pericapsular fibroinflammatory changes with thickening of the joint capsule at the axillary pouch (≥4 mm) or the rotator interval, along with thickening of the coracohumeral ligament (≥4 mm on MR arthrography) and obliteration of the subcoracoid fat triangle (Fig. 10.10) [25, 26]. According to a recent study, capsular thickness on MRI in the humeral portion of the axillary recess correlates with pain intensity and is greatest at the first of four clinical stages; obliteration of the subcoracoid fat triangle is also more frequent in the earlier stages [27].

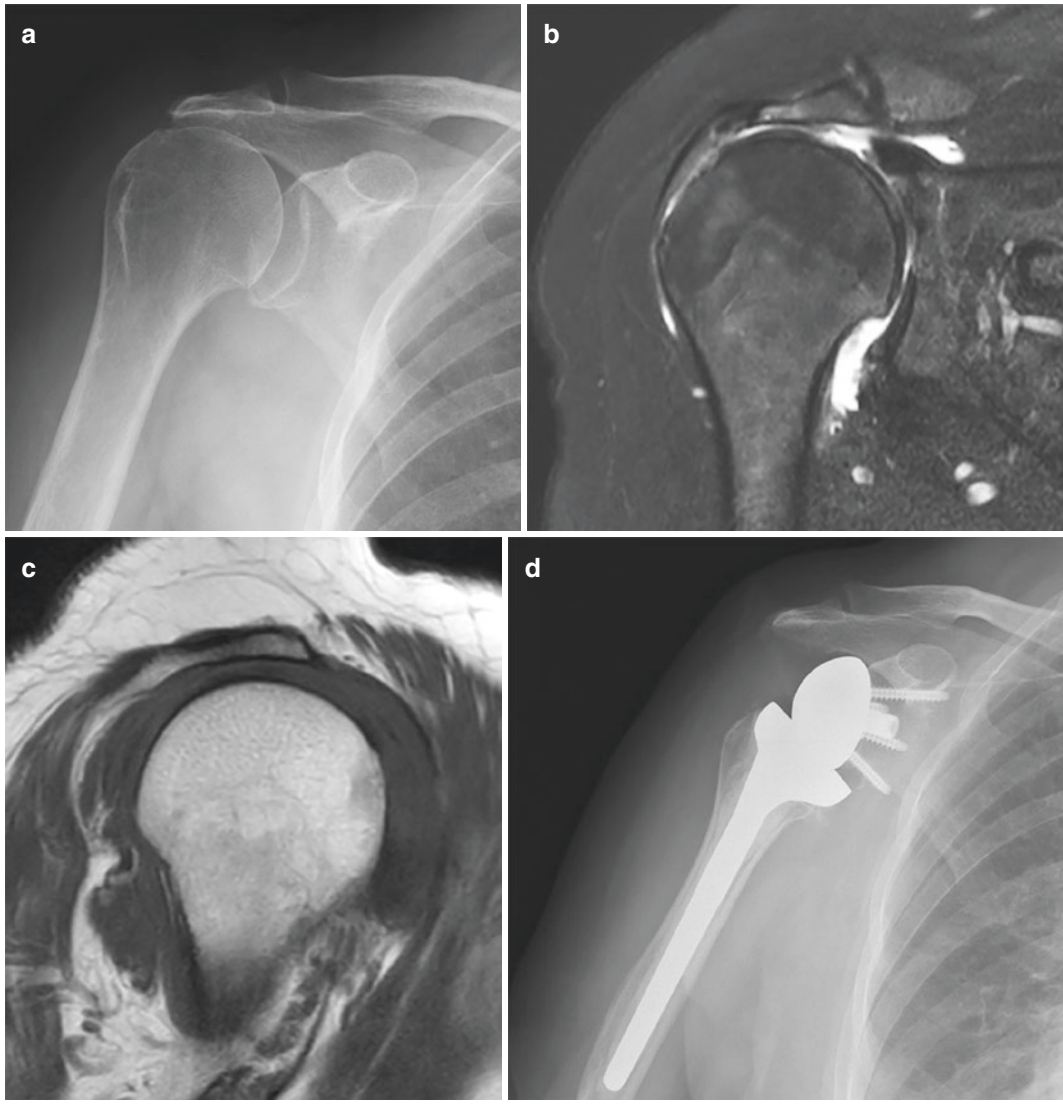

Fig. 10.8 Anteroposterior radiograph in external rotation (**a**), coronal oblique fat-saturated T2-weighted (**b**) and sagittal oblique T1-weighted (**c**) MR images of a 77-year-old woman show a decreased acromiohumeral distance due to a chronic massive rotator cuff tear, "femoralization" of the humeral head (**a**, **b**), and "acetabularization" of the coracoacromial arch (**c**), findings characteristic of rotator cuff tear arthropathy. Later, the patient underwent reverse total shoulder arthroplasty (**d**)

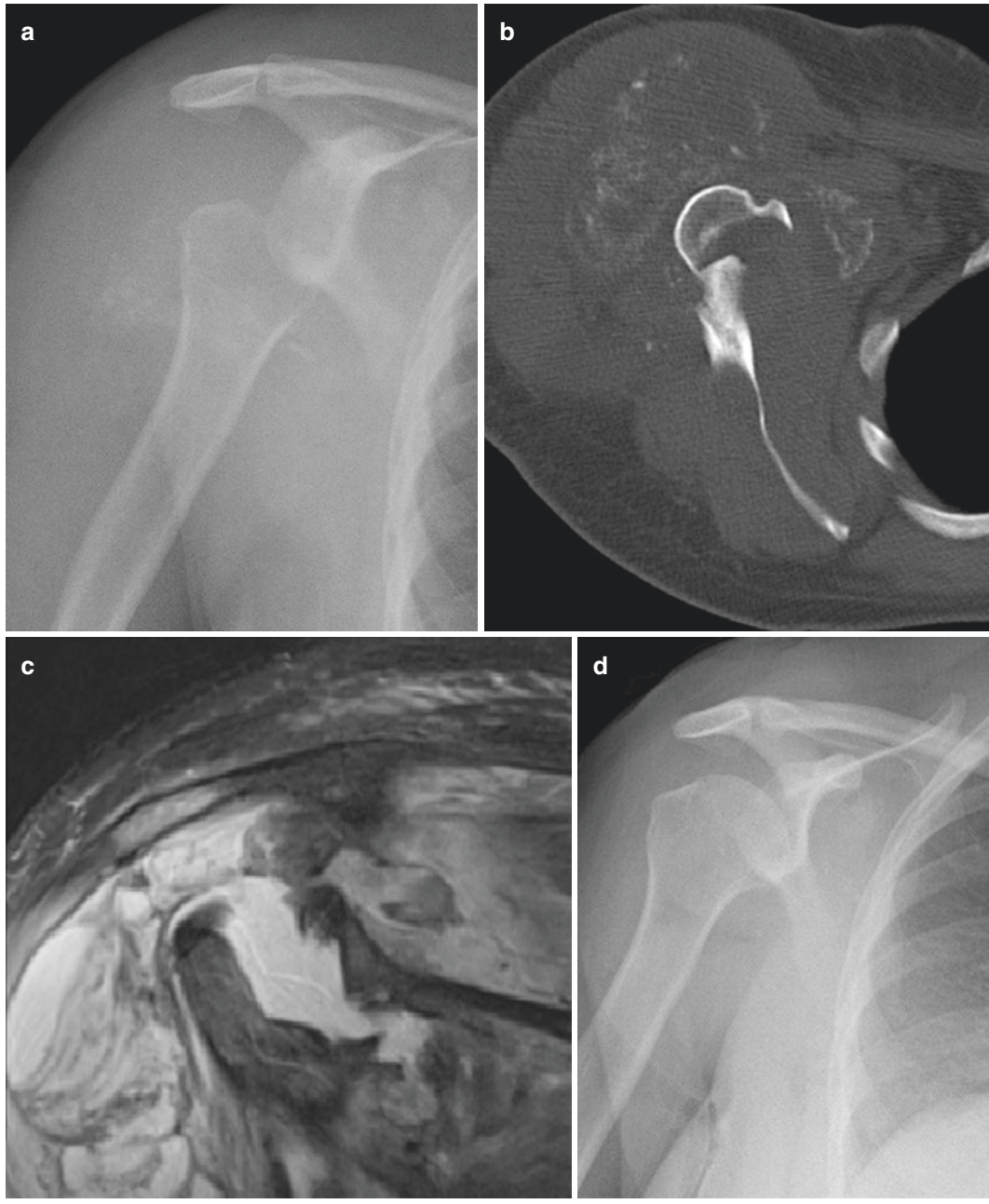

Fig. 10.9 Anteroposterior (AP) radiograph (**a**), transverse CT (**b**), and coronal (**c**) fat-saturated T2-weighted MR images show destruction of the glenohumeral joint and a large effusion with calcifications (**a**, **b**) in a 53-year-old woman, who presented with right shoulder pain and swelling. Active range of motion was severely limited. She had had no recent trauma to the shoulder area. Joint aspirate revealed hydroxyapatite crystals. An AP chest radiograph from 7 months earlier (**d**) was unremarkable for this region. Current condition of the patient is therefore consistent with a "Milwaukee shoulder." (Case courtesy of Zeynep Maraş Özdemir, MD, Malatya, Turkey)

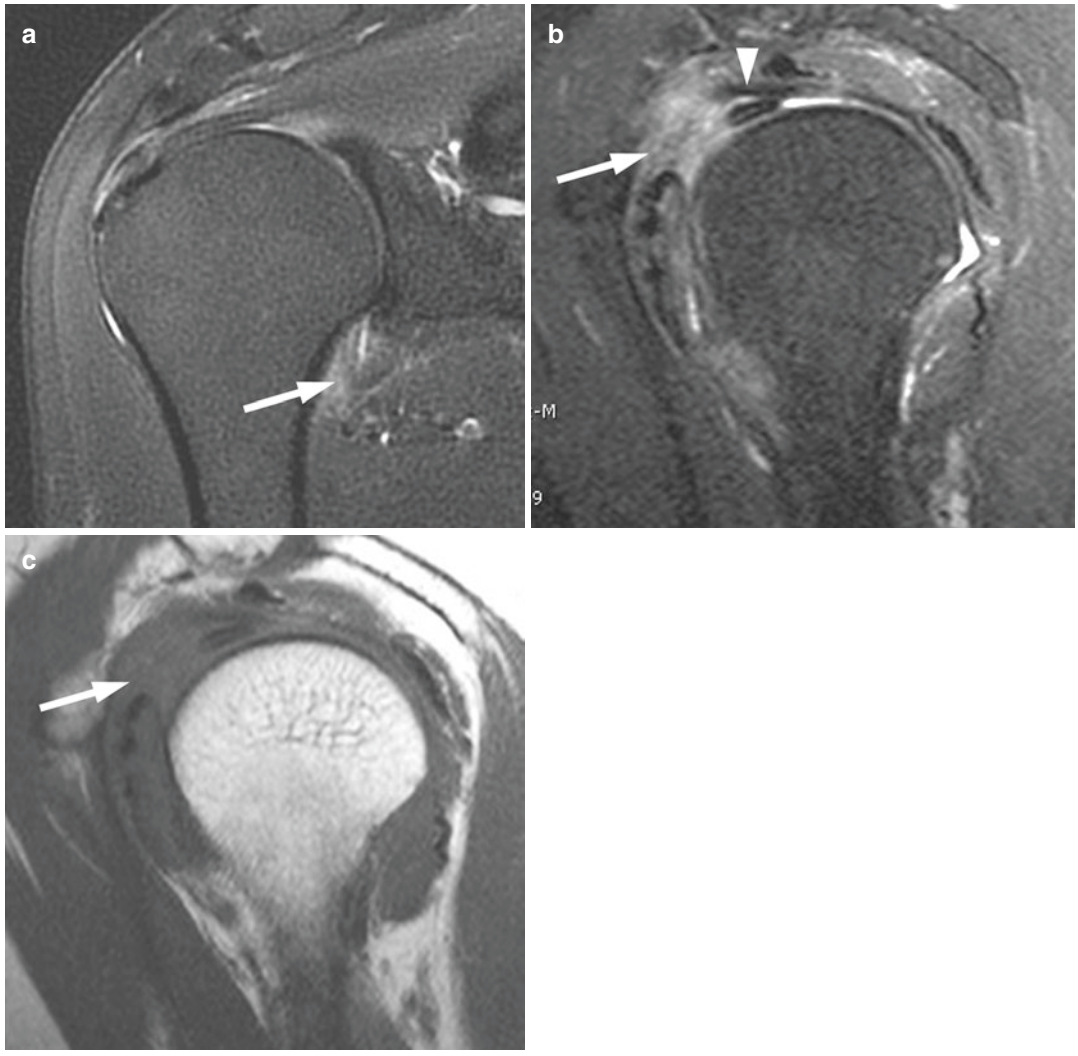

Fig. 10.10 Coronal oblique (**a**) and sagittal oblique (**b**) fat-saturated T2-weighted, and T1-weighted (**c**) MR images show thickening and edema of the joint capsule (inferior glenohumeral ligament) at the axillary pouch (**a**, *arrow*), and obliteration of the subcoracoid fat triangle by fibroinflammatory changes (*arrows,* **b**, **c**). The coracohumeral ligament is also mildly thickened (*arrowhead,* **b**). All of these findings are consistent with adhesive capsulitis

10.3.5 Calcific Tendinitis

Calcific tendinitis is characterized by the deposition of hydroxyapatite crystals within the tendons, most commonly of the rotator cuff. Patients are usually middle aged (between 30 and 60 years). Although this condition is usually self-healing with spontaneous resolution of the calcific deposits and surrounding inflammation over time, it may cause chronic moderate-to-marked pain with functional disability.

Magnetic resonance imaging exquisitely shows calcific deposits surrounded with soft tissue or bone inflammation. It is important to correlate the findings on MRI with radiography as small deposits might be subtle. For small deposits at the distal aspects of rotator cuff tendons, T1-weighted sagittal images are especially useful as tendons at this location are otherwise susceptible to the so-called magic angle phenomenon and would not usually display the hypointensity that could have masked such deposits. The novel

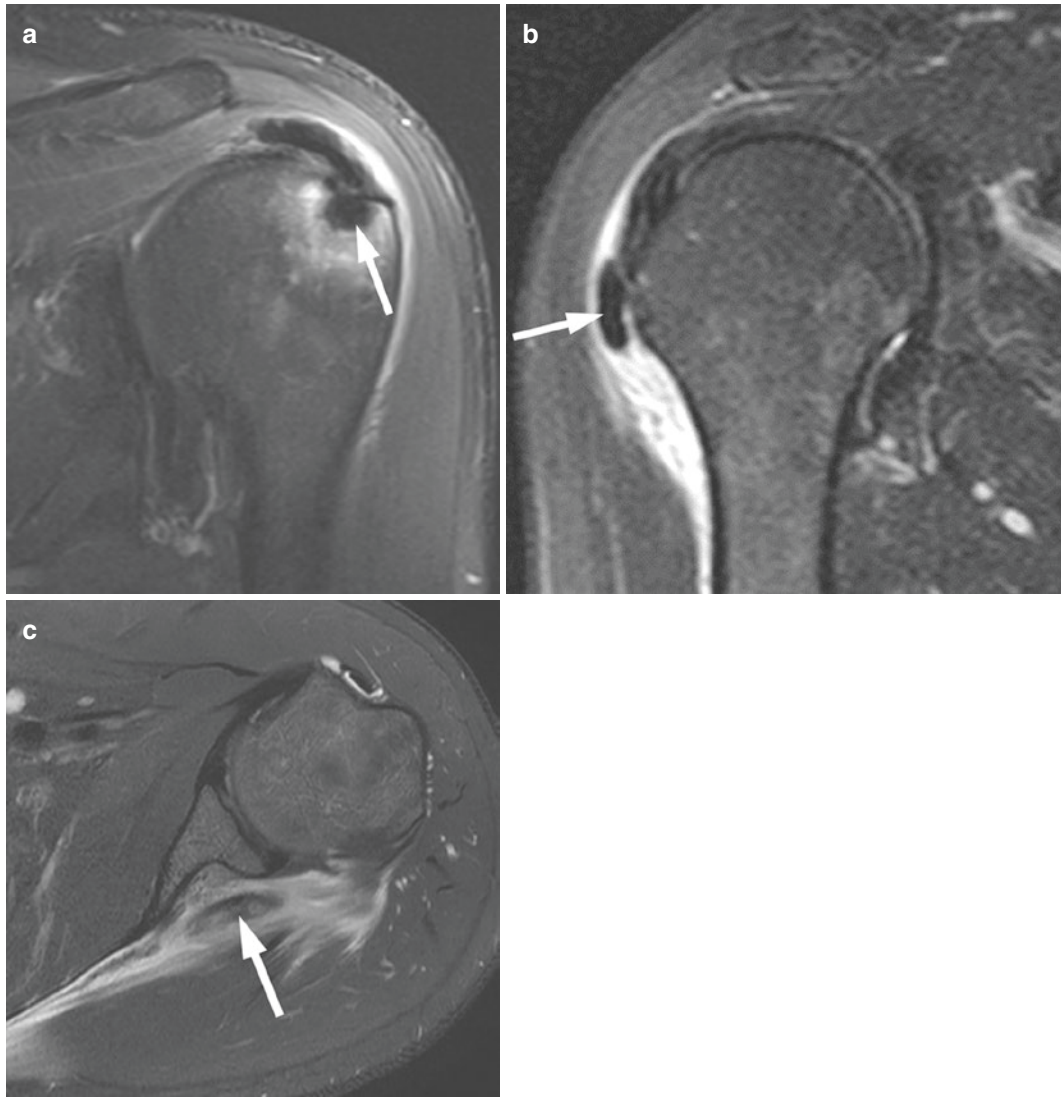

Fig. 10.11 Coronal oblique (**a**, **b**) and transverse (**c**) fat-saturated T2-weighted MR images show in three different patients migration of the calcific tendinitis deposits (*arrows*) into the humeral head, subdeltoid bursa, and infraspinatus muscle belly, respectively. Active inflammation surrounds the migrated deposits in each case

ZTE sequence also exquisitely displays such calcifications on MRI.

Migration of the calcific deposits into the bursae, humerus, and into the muscle belly can also occur and is easily depicted on MRI or CT (Fig. 10.11). Such migrated deposits and their surrounding inflammation can also subside over time.

Ultrasonographic appearance of calcific deposits are classified as hard (hyper-reflexive nodule with a well-circumscribed dorsal acoustic shadow), soft (well-circumscribed, homogeneous hyperechoic foci without posterior shadow), and fluid (hyperechoic peripheral rim with hypoechoic/anechoic center) [28]. Ultrasonography-guided percutaneous irrigation of calcific deposits is a valid treatment option as it is less invasive, quicker and with less post-procedural complication in comparison to arthroscopic removal (Fig. 10.12) [28]. Although different US-guided techniques and approaches have been reported using one or two needles of different sizes to remove calcium, no definite evidence exists in favor of using a specific size or number of needles [28].

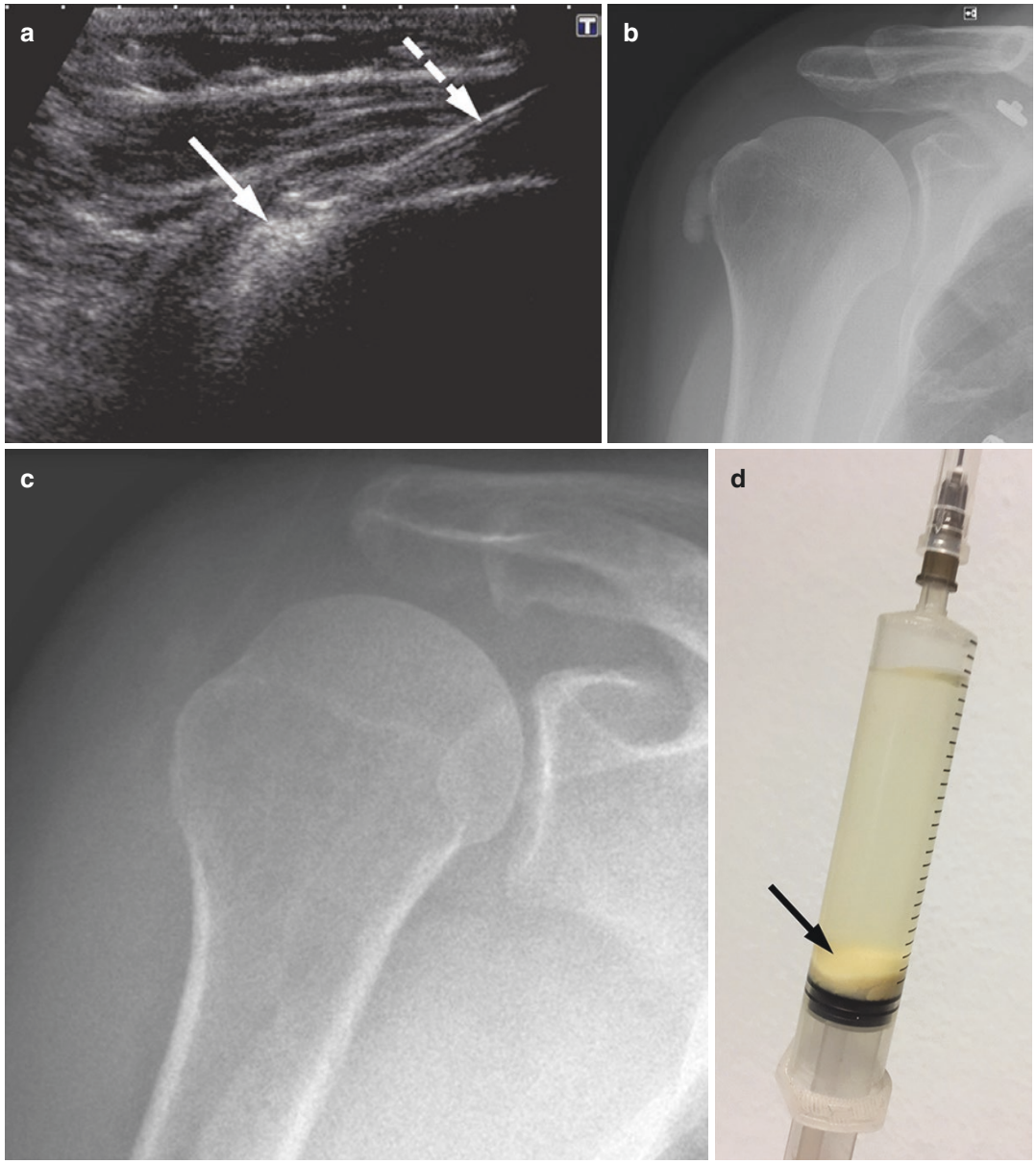

Fig. 10.12 Ultrasonography-guided percutaneous irrigation (**a**) of a calcific deposit (*arrow*) that migrated into the subdeltoid bursa in a 71-year-old woman (needle, *dashed arrow*). Grashey projection radiographs before (**b**) and after (**c**) the procedure show nearly complete removal of the calcific deposit. Calcium deposits layer (*arrow,* **d**) in the syringe filled with the fluid that was withdrawn after irrigation with physiologic saline

10.4 Imaging in Shoulder Instability

Radiography is the first-line imaging tool in the assessment of shoulder instability. In the acute setting, radiographs readily show the dislocation. Humeral head and glenoid fractures that are frequently associated with shoulder dislocations are also displayed on the standard trauma series, which usually comprises an AP view (neutral or with internal/external rotation), the scapular Y view, and the axillary view (or one of its modifications). Nevertheless, CT with 3D reconstructions is widely used to quantify bone stock in deciding and planning surgery. Magnetic resonance imaging is the

preferred cross-sectional imaging modality for the comprehensive assessment of bone and soft tissue lesions. Although MR-arthrography has little or no role in the acute setting (because of the usual presence of a joint effusion already creating an arthrographic effect), it exquisitely demonstrates in later stages capsulolabral as well as bony injury and rotator cuff tendon tears that might be associated with shoulder dislocation. MR-arthrography has a sensitivity of 88%–96% and a specificity of 91%–98% in the evaluation of glenoid labrum lesions [29]. In the last decade, the widespread availability of 3 T with improved image quality has somewhat decreased the use of MR-arthrography.

10.4.1 Anterior Instability

Concomitant bone injuries of the glenoid and humeral head, which are detected in up to 80% of patients with anterior shoulder instability, predispose to recurrent episodes of anterior shoulder dislocation with a cumulative effect depending on size and location [29]. Both posterolateral humeral head impaction fracture (Hill-Sachs lesion) and, more importantly, anterior glenoid rim fracture are important to characterize and quantify preoperatively because of their importance in prognosis and surgical guidance.

Soft tissue lesions of anterior shoulder instability include Bankart, Perthes, anterior labroligamentous periosteal sleeve avulsion (ALPSA), glenoid labrum articular disruption (GLAD), and humeral avulsion of the (inferior) glenohumeral ligament (HAGL) lesions (Fig. 10.13). The most commonly torn rotator cuff tendon in anterior shoulder dislocation is the subscapularis [29]. In soft tissue Bankart lesions, which occur at the anteroinferior aspect of the glenoid (3–6 o'clock), both the labrum and its capsular insertion along with the glenoid periosteum are torn, and the labrum may be partially or completely detached from the glenoid rim. In a recent study, Bankart tears demonstrated on MR-arthrography fluid signal more often (92%) on T2-weighted images than gadolinium-based contrast signal (76%) on T1-weighted images, suggesting that resynovialization could cause joint fluid to be trapped beneath the tear [29, 30]. Perthes lesion denotes a non-displaced tear of the anteroinferior labrum and the inferior glenohumeral ligament (IGHL), whereby the glenoid periosteum remains intact. Since the labrum remains anatomically positioned, this lesion may be overlooked at arthroscopy. With the addition of ABER sequence to MR-arthrography, Perthes lesions become often more conspicuous (Fig. 10.3) [29]. GLAD lesion refers to the presence of articular cartilage injury (in the form of fibrillation, erosion, impaction, detachment, or delamination) adjacent to a non-displaced tear of the anteroinferior labrum. The periosteum and the IGHL usually remain intact. Both the HAGL lesion, characterized by humeral avulsion of the IGHL, and glenoid avulsion of the IGHL are exquisitely shown on MRI or MR-arthrography. Either type of these lesions can sometimes present with a detached bony fragment at the humeral or glenoid side (radiography correlation is particularly useful since MRI might not readily show small bony fragments). A "floating" anterior IGHL results from the rare occurrence of a HAGL lesion with a concomitant anteroinferior capsulolabral tear [29].

It is more important and relevant for the radiologist to describe the injured structures and the extent of injury along with the presence of any displacement rather than to furnish a pinpoint term-based diagnosis. Although anatomic variants such as a sublabral foramen (a gap between the anterosuperior labrum and the glenoid) and the Buford complex (cordlike thickening of the middle glenohumeral ligament in the absence of the anterosuperior labrum) can be seen on shoulder MRI, it is important to realize that there is an association between these conditions and a superior labral tear likely due to increased stress on the bicipitolabral complex [9].

In anterior and anteroinferior dislocations, the Pico method, which utilizes a best-fit circle drawn on the glenoid joint surface on CT reconstructions showing the glenoid *en face*, accurately quantifies glenoid bone loss and is associated with recurrent dislocation when above 20% (Fig. 10.14) [29].

With the better visibility of rotator cuff insertion than on CT and the possibility of producing CT-like images with the recently introduced ZTE sequence [7, 8], MRI affords a better feasibility of determining whether the bipolar (i.e., humeral and glenoid) bone lesions (Hill-Sachs and bony

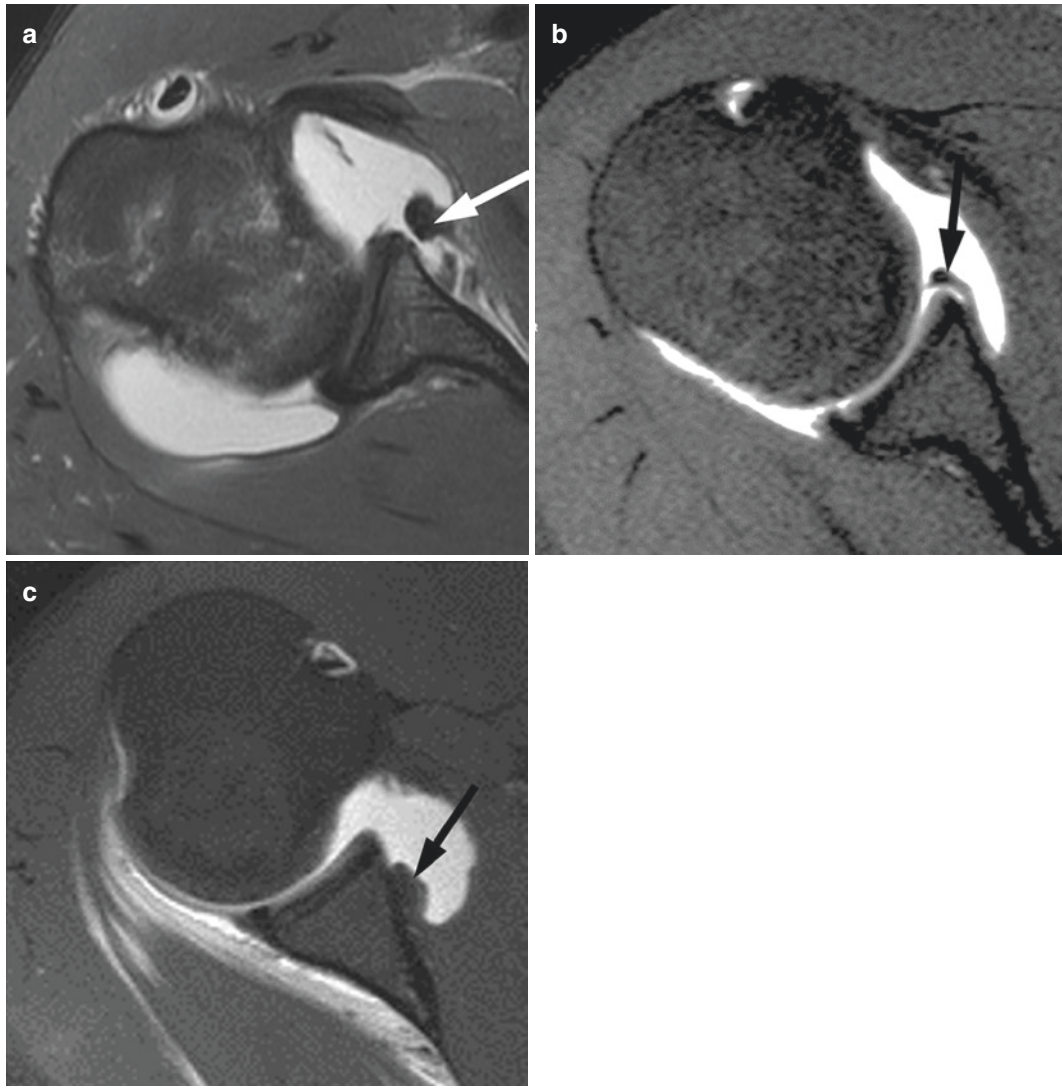

Fig. 10.13 Transverse fat-saturated T2-weighted MR (**a**) and fat-saturated T1-weighted MR-arthrography (**b**, **c**) images show Bankart, Perthes, and anterior labroligamentous periosteal sleeve avulsion (ALPSA) lesions (*arrows*) in three different patients. Conventional MRI in the patient with Bankart lesion (**a**) was obtained shortly after trauma and shows moderate joint effusion, obviating the need for an MR-arthrography (**b**, **c**)

Bankart lesions, respectively) are "on-track" or "off-track" [29]. Bipolar bone lesions are considered "off-track" and at risk for engagement (i.e., recurrent dislocation and the need for revision surgery) if the Hill-Sachs interval (HSI) is greater than the glenoid track. HSI is composed of the Hill-Sachs impaction fracture width plus the intact bone bridge width between the Hill-Sachs lesion and the medial edge of the rotator cuff tendon insertion on transverse MR images. The glenoid track is given by the formula: $0.83 \times (D–d)$, where D represents the diameter of the intact glenoid as outlined in a circle *en face* as in the Pico method, and d represents the amount of anterior glenoid bone loss (both in millimeters). Bone lesions associated with anterior instability are considered on-track and not at risk for engagement (and recurrent dislocation) if the HSI is less than the glenoid track [29, 31]. The recommended treatment strategy for on-track and off-track lesions depending on the glenoid bone loss being $<25\%$ or $\geq 25\%$ is different [31].

Fig. 10.14 Imaging-based pre-operative assessment of the glenoid stock utilizes a best-fit circle drawn on the glenoid joint surface on a three-dimensional CT reconstruction showing the glenoid *en face*, which in this patient also features a bony Bankart lesion (*arrow*)

10.4.2 Posterior Instability

The much less common condition of posterior shoulder instability also has imaging findings. Radiographs can show an engaged posterior shoulder dislocation or its sequelae. Radiographic findings on AP projection include the absence of normal overlap of the humeral head and glenoid, the "lightbulb sign," which denotes the fixed internal rotation of the humerus, and the "trough sign," which refers to the double contour of the medial humeral head representing the long axis of a reverse Hill-Sachs fracture parallel to the normal medial cortex (Fig. 10.15) [14]. Reverse Hill-Sachs lesion (also known as McLaughlin lesion), which is an impaction fracture at the anteromedial aspect of the humeral head and reverse bony Bankart lesion at the posteroinferior glenoid rim are usually better seen on CT and MRI. If more than 30% of the articular surface is involved in a reverse Hill-Sachs lesion or when there are associated injuries of the posterior capsulolabral ligamentous structures, the risk of instability increases [32]. Soft tissue lesions associated with posterior dislocation include reverse Bankart lesion, posterior labrocapsular

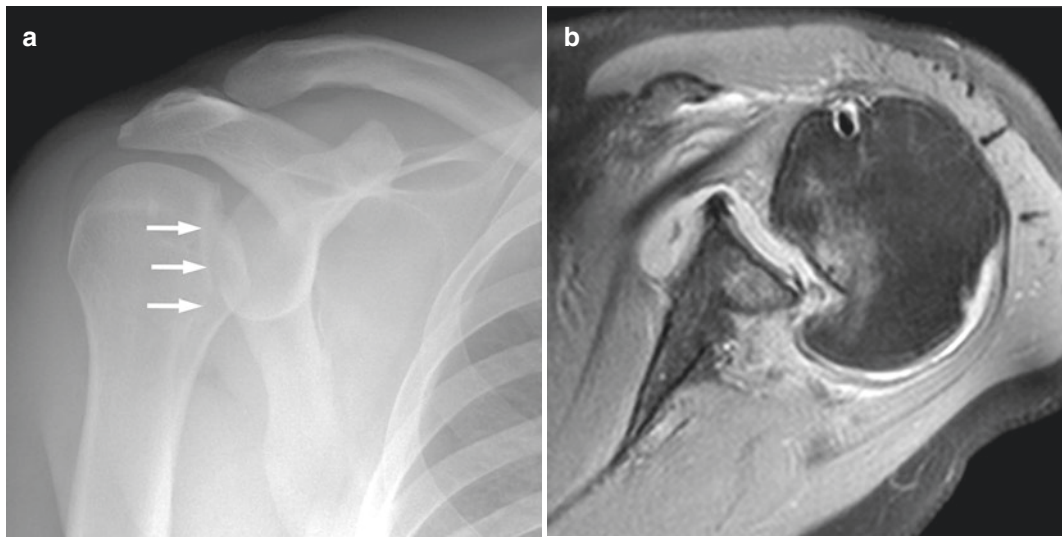

Fig. 10.15 A neutral anteroposterior radiograph of the shoulder (**a**) displays the "trough sign," created by the double contour of the medial humeral head representing the long axis of a reverse Hill-Sachs fracture parallel to the medial cortex (*arrows*). Transverse MR image (**b**) in another patient, who likewise sustained a posterior shoulder dislocation, shows an engaging reverse Hill-Sachs lesion

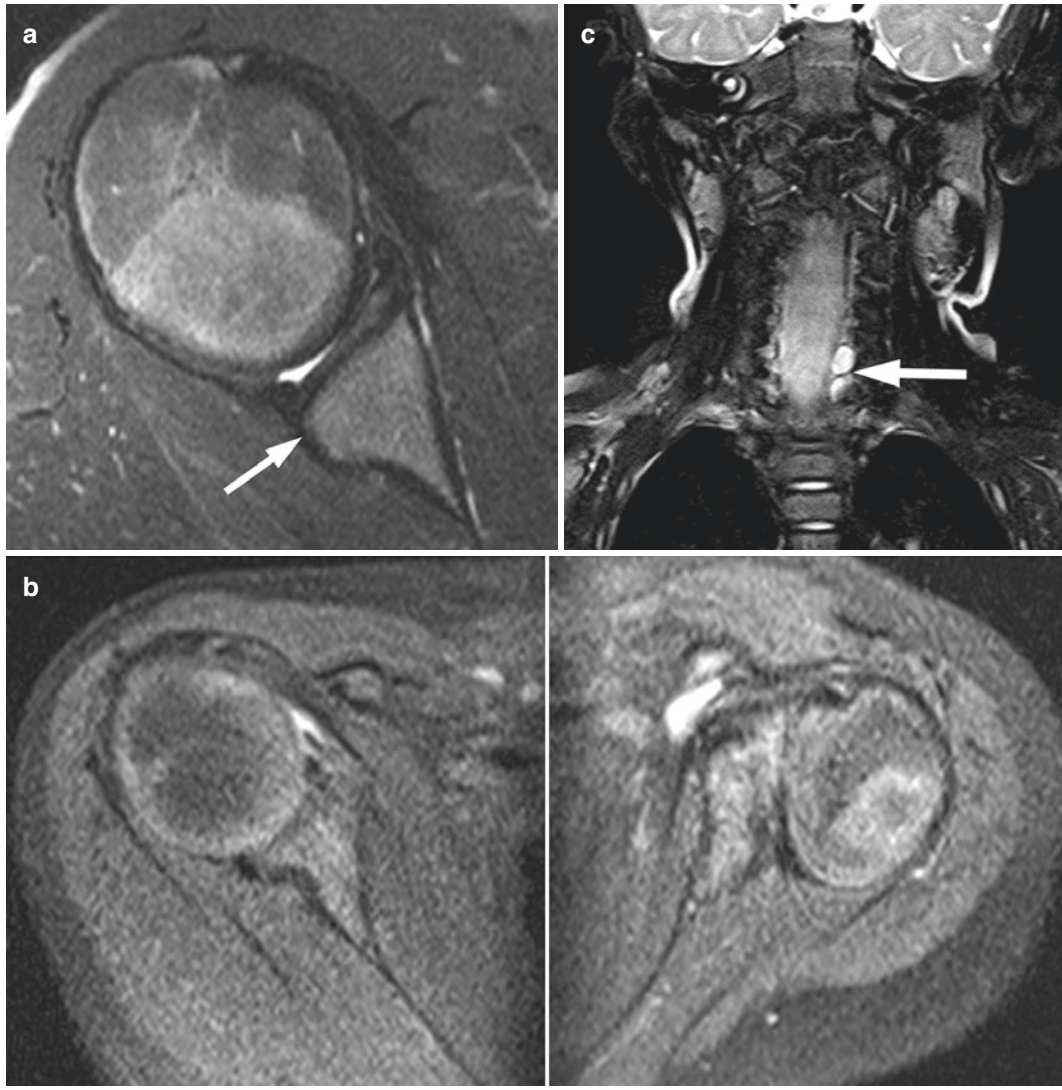

Fig. 10.16 Transverse fat-saturated T2-weighted MR image (**a**) shows a dysplastic posterior glenoid (*arrow*) in a young adult. A composite fat-saturated proton-density MR image showing both shoulders (**b**) and a coronal T2-weighted MR image (**c**) show left-sided glenohumeral dysplasia due to obstetric brachial plexus palsy in an infant with lower cervical spinal nerve root avulsions that resulted in meningeal cysts/diverticula (*arrow,* **c**). Note retroversion of the left glenoid cavity with subluxation of the left humeral head and atrophy of the rotator cuff muscles (**b**)

periosteal sleeve avulsion (POLPSA), and Kim lesion, which is a superficial tear between the posterior glenoid labrum and glenoid articular cartilage without labral detachment.

Glenoid dysplasia, which is a congenital abnormality likely resulting from underdevelopment of the inferior glenoid ossification center, predisposes to posterior instability. In this condition, the scapular neck and the humeral head can be hypoplastic and humeral neck can display varus deformity. MRI shows a dysplastic posterior glenoid with compensatory hypertrophy of the posterior cartilage and/or labrum (Fig. 10.16a). Glenohumeral dysplasia due to obstetric brachial plexus palsy produces MRI findings that can be observed in infants as young as 3 months [33] and include retroversion of the glenoid cavity, developmental delay, posterior translation/subluxation of the humeral head, and atrophy of the rotator cuff muscles (Fig. 10.16b, c).

10.5 Imaging in Some Other Shoulder Conditions

10.5.1 Long Head Biceps Tendon Lesions

Long head of the biceps tendon (LHBT) lesions occur most commonly at the subacromial part of this tendon (i.e., at the rotator interval) and they are an important pain generator. Since clinical tests are often equivocal, imaging plays an important role in ascertaining these lesions. One commonly encountered lesion on shoulder MRI is LHBT tendonosis either by itself or in combination with rotator cuff conditions. A systematic review of the literature showed that chronic LHBT tendinopathy is associated with chronic supraspinatus tendinopathy [34]. It is imperative to follow the LHBT on all three MRI planes as it courses around the humeral head to insert on the supraglenoid tubercle (Fig. 10.17).

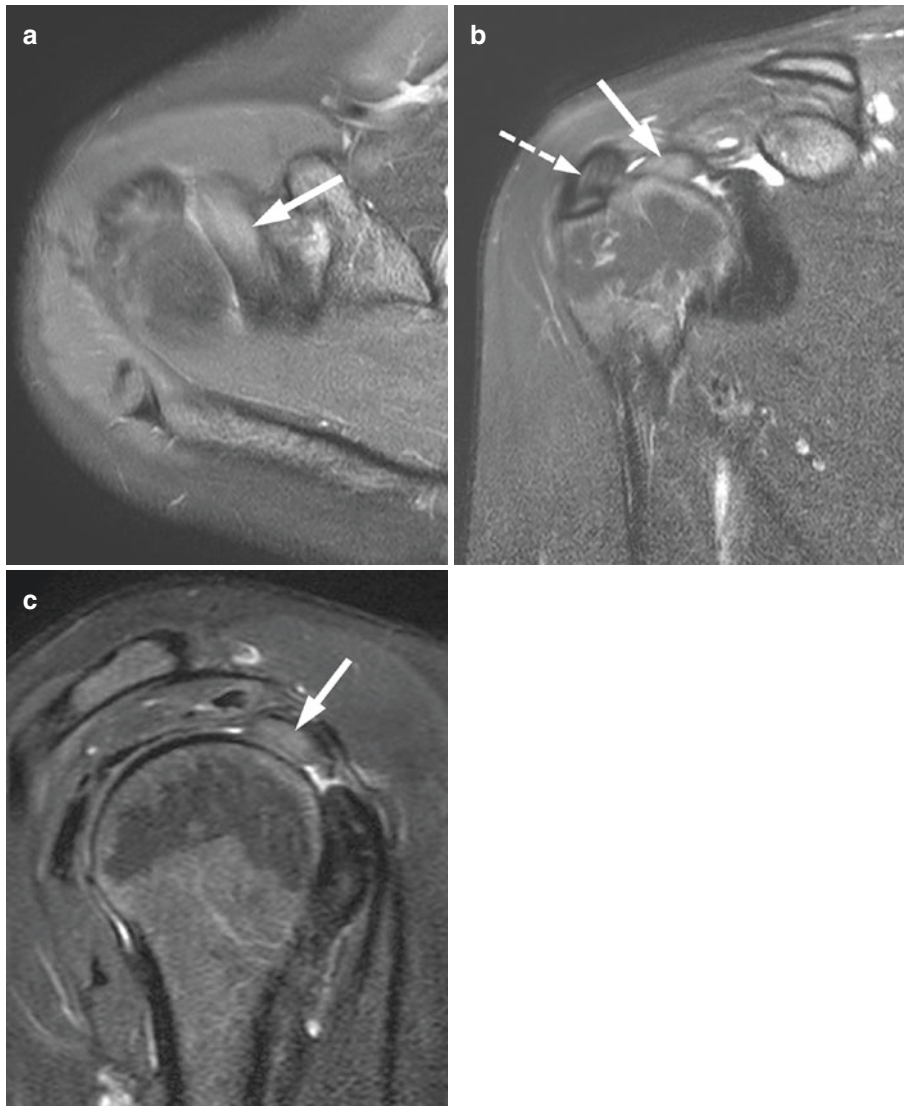

Fig. 10.17 Transverse (**a**), coronal oblique (**b**), and sagittal oblique (**c**) fat-saturated T2-weighted MR images show tendonosis of the long head biceps tendon (LHBT, *arrows*). Note also tendonosis of the supraspinatus tendon (*dashed arrow,* **b**)

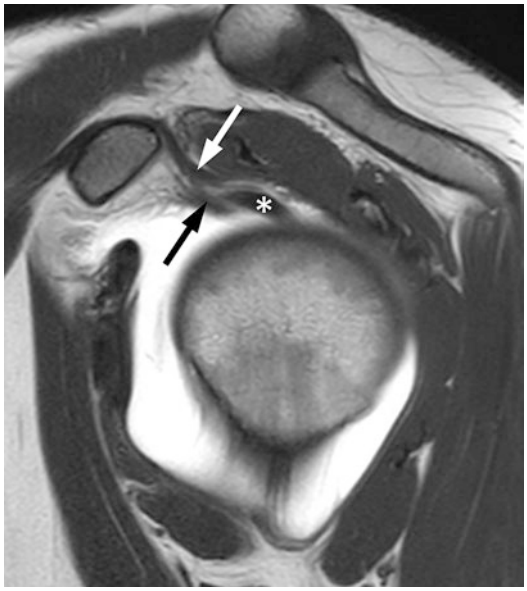

Fig. 10.18 Biceps pulley and the intraarticular portion of the long head biceps tendon (LHBT). Sagittal T1-weighted MR-arthrography image shows the coracohumeral ligament (CHL, *white arrow*) and the superior glenohumeral ligament (SGHL, *black arrow*) anteriorly enveloping the biceps tendon long head (*asterisk*)

MR-arthrography superbly shows the LHBT and its supporting structures (mainly the biceps pulley) [35]. Biceps pulley is defined either somewhat narrowly as the ligamentous sling consisting of the CHL and SGHL (Fig. 10.18) or more broadly as the entire stabilizing structure for LHBT consisting of the CHL, SGHL, and upper border of the subscapularis tendon as well as the anterior border of the supraspinatus tendon. Biceps pulley guides and stabilizes the LHBT during its deflection from the intraarticular horizontal segment to the extraarticular vertical portion. It prevents medial subluxation of the LHBT, along with which it also stabilizes the shoulder against superior translation. The latter is especially important in patients with supraspinatus tendon tears.

It is important to realize that shape variations and slightly eccentric position of LHBT within the humeral groove on MRI can also be seen in healthy volunteers [36]. Medial subluxation of the LHBT usually implies a subscapularis tendon lesion and biceps pulley tear. This finding on MR-arthrography is highly specific but not very sensitive [35]. The signs of nonvisibility or discontinuity of the SGHL and caudad and/or anterior displacement of the LHBT relative to the subscapularis tendon on MR-arthrography have higher sensitivity (with quite high specificity) for biceps pulley tears.

Biceps pulley lesions are often associated with supraspinatus and/or subscapularis tendon tears and SLAP tears. Therefore, all relevant structures need to be carefully assessed on MR-arthrography images. LHBT can dislocate superficial or deep to the subscapularis tendon, depending on which pulley components are torn (Fig. 10.19) [37].

10.5.2 Distal Clavicular Osteolysis

As a recognized cause of shoulder pain, distal clavicular osteolysis can mimic physical examination findings—as well as symptoms—of rotator cuff injury and labral tears, with which it can coexist [38]. It typically follows an acute traumatic incident or, more commonly, chronic repetitive stress to the acromioclavicular joint (usually related to weightlifting and overhead sports). Initial radiographs may be normal; later periostitis, resorption, and/or osteopenia at the distal clavicle can be seen. This condition is seen on MRI as a stress reaction in the form of bone marrow edema/contusion sometimes accompanied with a frank stress fracture (Fig. 10.20a), before characteristic osteolysis of distal clavicle (Fig. 10.20b) is visible on conventional radiographs.

10.5.3 Nerve Compression or Entrapment

Suprascapular nerve compression or entrapment at the levels of suprascapular or spinoglenoid notches can result in denervation changes at the supraspina-

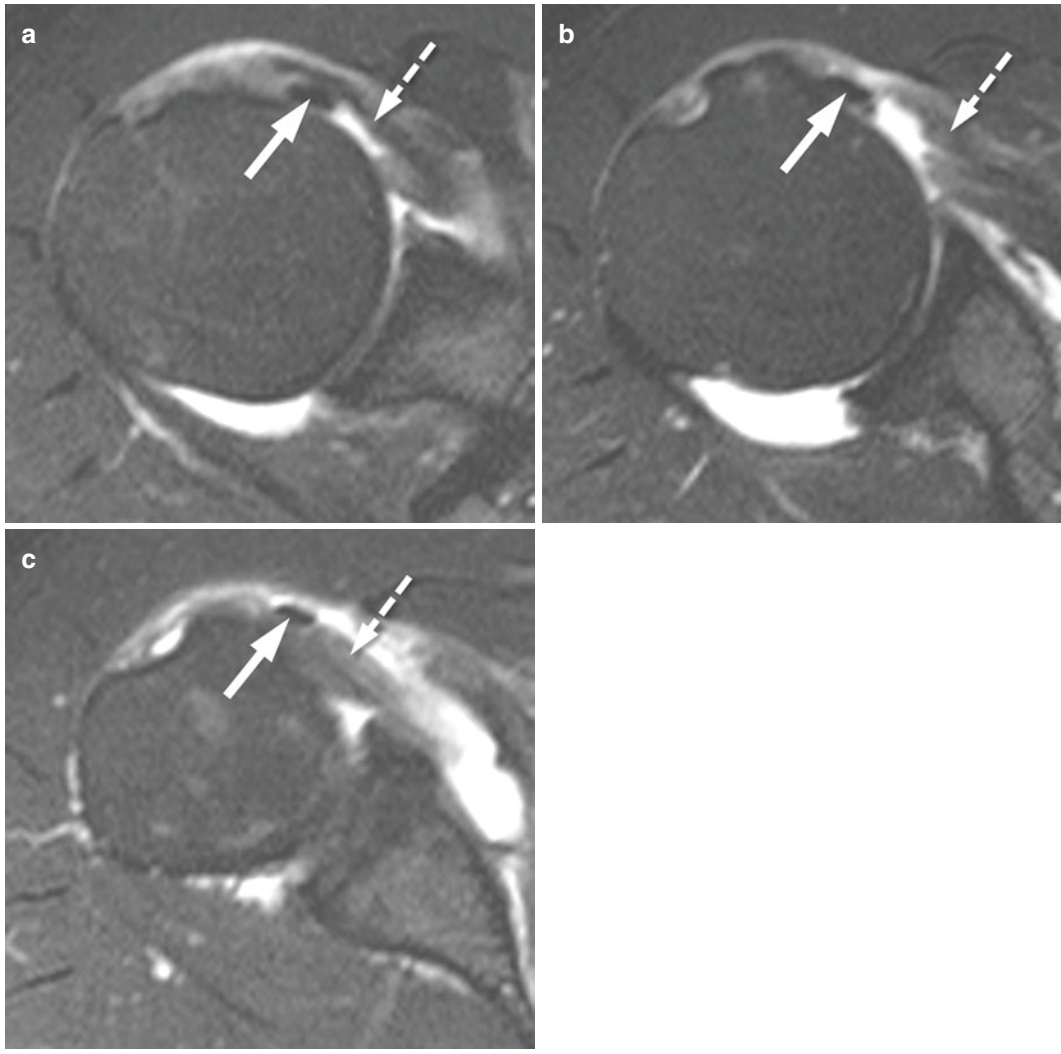

Fig. 10.19 Craniocaudally consecutive transverse fat-saturated proton-density MR images (**a**–**c**) show a medially dislocated long head biceps tendon (LHBT, *arrows*) crossing the torn distal portion of the subscapularis tendon (*dashed arrows*)

tus and infraspinatus muscle bellies or only infraspinatus muscle belly, respectively (Fig. 10.21).

Teres minor denervation changes on MRI have an incidence of 3% (Fig. 10.22) [39]. Quadrilateral space syndrome results from the compression of axillary nerve or one of its major branches in the quadrilateral space, affecting the deltoid and/or teres minor. Axillary nerve is susceptible to injury not only in its segment at the quadrilateral space but also as it courses around the glenoid and posterior capsule and can be injured by repetitive microtrauma associated with humeral head instability [13]. Preservation of teres minor muscle bulk and function is an important prognostic factor in reverse shoulder arthroplasty and tendon transfers [40].

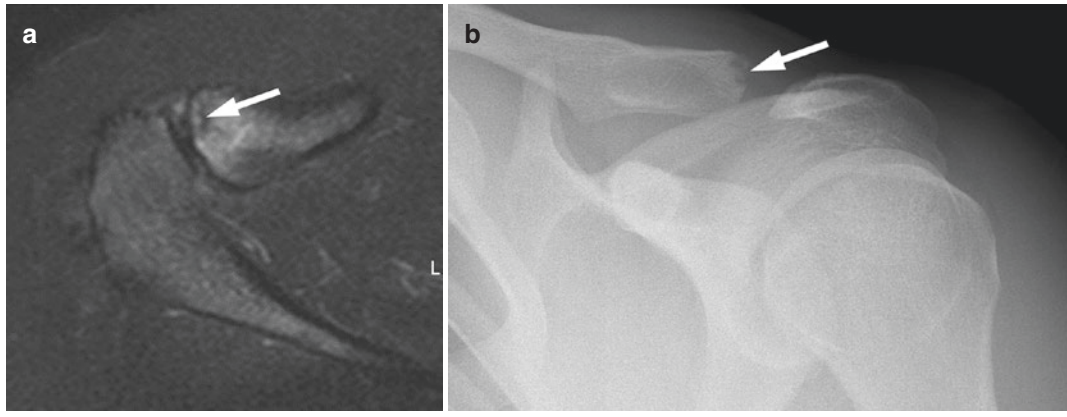

Fig. 10.20 Transverse fat-saturated T2-weighted MR image (**a**) displays a subchondral insufficiency fracture (*arrow*) surrounded with bone marrow edema-like signal. Anteroposterior radiograph in internal rotation (**b**) shows resorptive changes (*arrow*) characteristic of distal clavicular osteolysis in another patient who displayed distal clavicular bone marrow edema-like changes on MRI

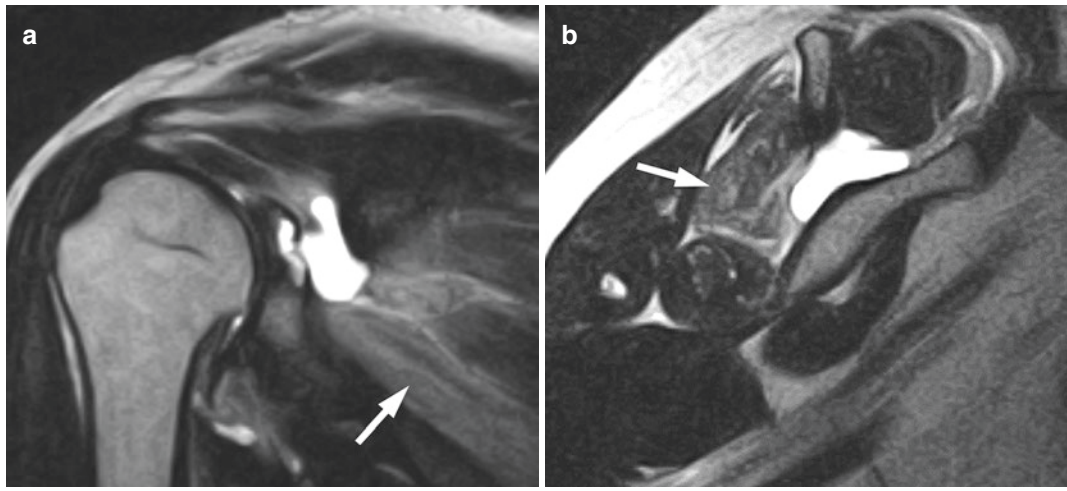

Fig. 10.21 Coronal oblique (**a**) and sagittal oblique T2-weighted (**b**) MR images show a paralabral cyst centered at the level of the spinoglenoid notch causing suprascapular nerve compression that resulted in denervation changes at the infraspinatus muscle (*arrows*), sparing the supraspinatus

Fig. 10.22 Sagittal oblique T1-weighted MR image shows isolated atrophy of the teres minor (*arrow*) with Goutallier stage 2 (or Fuchs grade 2) fatty infiltration in a 43-year-old man who sustained a fall several months earlier. A branch of the axillary nerve might have been injured

10.5.4 Enchondroma

Differentiating an enchondroma from a low-grade chondrosarcoma affecting the appendicular skeleton (proximal to the metacarpals and metatarsals) is challenging even for pathologists, who take into account parameters such as cellularity, number of mitoses, and cellular atypia. Some radiological features can be helpful in these instances. Deep endosteal scalloping more than two-thirds of the cortex is associated with an increased risk of malignancy (Fig. 10.23) [41]. Other clinical and imaging features that favor chondrosarcoma include pain related to the lesion, cortical destruction and soft-tissue mass, periosteal reaction, and marked uptake of radionuclide (greater than the anterior iliac crest) at bone scintigraphy. MRI is the best imaging modality to follow up cartilage matrix lesions after treatment with curettage and cementing.

10.6 Conclusion

Radiological assessment is essential in addressing a wide range of shoulder problems. The combination of radiography with MRI and/or MR-arthrography is the most commonly used set of imaging tools. Computed tomography is useful for further assessment of fractures and dislocations and helps in surgical planning. Zero echo-time (ZTE) imaging, which is a recently introduced MRI sequence producing CT-like images, may obviate the need to obtain additional or complementary CT for glenoid stock estimation and glenoid track assessment. CT-arthrography needs to be considered whenever there is a contraindication for MR-arthrography. Ultrasonography is used in the shoulder mostly for the evaluation of bursitis, rotator cuff and LHBT abnormalities, as well as for guidance during MR- and/or CT-arthrography, and percutaneous irrigation of calcific tendinitis.

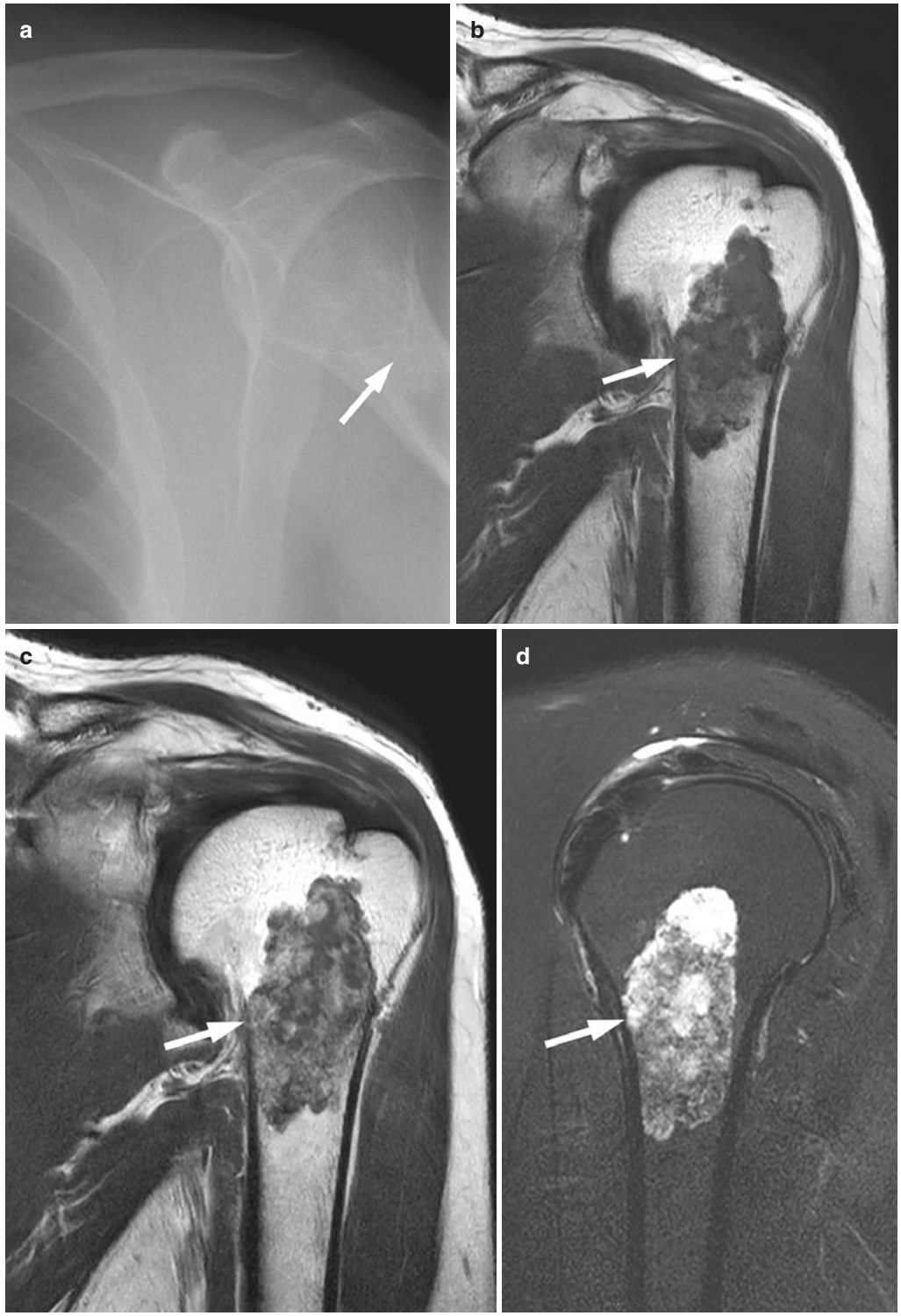

Fig. 10.23 An incidental lesion with stippled calcification in the proximal left humerus metaphysis was encountered on a posteroanterior chest radiograph (**a**). Coronal T1-weighted pre- (**b**) and post-contrast (**c**), and sagittal oblique fat-saturated T2-weighted (**d**) MR images show a lesion with chondroid matrix that features ring and arc type enhancement (**c**) and internal calcifications. The thinning of the cortex medially (*arrows,* **b**–**d**) suggests malignancy (i.e., low-grade chondrosarcoma)

References

1. Aydıngöz Ü, Canbulat N, Demirhan M. Radiological assessment of the shoulder region. Turk J Phys Med Rehabil. 2014;60:S68–77. https://doi.org/10.5152/tftrd.2014.36744.
2. Loriaud A, Bise S, Meyer P, Billaud A, Dallaudiere B, Silvestre A, Pesquer L. Critical shoulder angle: what do radiologists need to know? Skeletal Radiol. 2020;49(4):515–20. https://doi.org/10.1007/s00256-019-03337-3.
3. Magarelli N, Milano G, Sergio P, Santagada DA, Fabbriciani C, Bonomo L. Intra-observer and interobserver reliability of the 'Pico' computed tomography method for quantification of glenoid bone defect in anterior shoulder instability. Skeletal Radiol. 2009;38:1071–5.
4. Combes D, Lancigu R, Desbordes de Cepoy P, Caporilli-Razza F, Hubert L, Rony L, Aubé C. Imaging of shoulder arthroplasties and their complications: a pictorial review. Insights Imaging. 2019;10(1):90. https://doi.org/10.1186/s13244-019-0788-5.
5. Omoumi P, Rubini A, Dubuc JE, Vande Berg BC, Lecouvet FE. Diagnostic performance of CT-arthrography and 1.5T MR-arthrography for the assessment of glenohumeral joint cartilage: a comparative study with arthroscopic correlation. Eur Radiol. 2015;25(4):961–9. https://doi.org/10.1007/s00330-014-3469-2.
6. Rhee RB, Chan KK, Lieu JG, Kim BS, Steinbach LS. MR and CT arthrography of the shoulder. Semin Musculoskelet Radiol. 2012;16(1):3–14. https://doi.org/10.1055/s-0032-1304297.
7. Breighner RE, Endo Y, Konin GP, Gulotta LV, Koff MF, Potter HG. Zero echo time imaging of the shoulder: enhanced osseous detail by using MR imaging. Radiology. 2018;286(3):960–6. https://doi.org/10.1148/radiol.2017170906.
8. de Mello RAF, Ma YJ, Ashir A, et al. Three-dimensional zero echo time magnetic resonance imaging versus 3-dimensional computed tomography for glenoid bone assessment. Arthroscopy 2020;36(9):2391–400. https://doi.org/10.1016/j.arthro.2020.05.042.
9. Motamedi D, Everist BM, Mahanty SR, Steinbach LS. Pitfalls in shoulder MRI: Part 1—normal anatomy and anatomic variants. AJR Am J Roentgenol. 2014;203(3):501–7. https://doi.org/10.2214/AJR.14.12848.
10. Motamedi D, Everist BM, Mahanty SR, Steinbach LS. Pitfalls in shoulder MRI: Part 2—biceps tendon, bursae and cysts, incidental and postsurgical findings, and artifacts. AJR Am J Roentgenol. 2014;203(3):508–15. https://doi.org/10.2214/AJR.14.12849.
11. Bunnell KM, Hemke R, Husseini JS, Torriani M, Huang SY, Bredella MA. Does MR arthrography cause intracranial gadolinium deposition? Skeletal Radiol. 2020;49(7):1051–6. https://doi.org/10.1007/s00256-020-03380-5.
12. Aydıngöz Ü, Maraş Özdemir Z, Ergen FB. Demystifying ABER (ABduction and External Rotation) sequence in shoulder MR arthrography. Diagn Interv Radiol. 2014;20(6):507–10. https://doi.org/10.5152/dir.2014.14117.
13. McCrum E. MR imaging of the rotator cuff. Magn Reson Imaging Clin N Am. 2020;28(2):165–79. https://doi.org/10.1016/j.mric.2019.12.002.
14. Goes PCK, Pathria MN. Radiographic/MR imaging correlation of the shoulder. Magn Reson Imaging Clin N Am. 2019;27(4):575–85. https://doi.org/10.1016/j.mric.2019.07.005.
15. Lawrence RL, Moutzouros V, Bey MJ. Asymptomatic rotator cuff tears. JBJS Rev. 2019;7(6):e9. https://doi.org/10.2106/JBJS.RVW.18.00149.
16. Connor PM, Banks DM, Tyson AB, Coumas JS, D'Alessandro DF. Magnetic resonance imaging of the asymptomatic shoulder of overhead athletes: a 5-year follow-up study. Am J Sports Med. 2003;31(5):724–7.
17. Adams CR, Brady PC, Koo SS, Narbona P, Arrigoni P, Karnes GJ, Burkhart SS. A systematic approach for diagnosing subscapularis tendon tears with preoperative magnetic resonance imaging scans. Arthroscopy. 2012;28(11):1592–600. https://doi.org/10.1016/j.arthro.2012.04.142.
18. Lunn JV, Castellanos-Rosas J, Tavernier T, Barthélémy R, Walch G. A novel lesion of the infraspinatus characterized by musculotendinous disruption, edema, and late fatty infiltration. J Shoulder Elbow Surg. 2008;17(4):546–53. https://doi.org/10.1016/j.jse.2007.11.016.
19. Somerson JS, Hsu JE, Gorbaty JD, Gee AO. Classifications in brief: Goutallier classification of fatty infiltration of the rotator cuff musculature. Clin Orthop Relat Res. 2016;474(5):1328–32. https://doi.org/10.1007/s11999-015-4630-1.
20. Zanetti M, Gerber C, Hodler J. Quantitative assessment of the muscles of the rotator cuff with magnetic resonance imaging. Invest Radiol. 1998;33(3):163–70.
21. Pierce JL, Nacey NC, Jones S, Rierson D, Etier B, Brockmeier S, Anderson MW. Postoperative shoulder imaging: rotator cuff, labrum, and biceps tendon. Radiographics. 2016;36(6):1648–71.
22. Eajazi A, Kussman S, LeBedis C, Guermazi A, Kompel A, Jawa A, Murakami AM. Rotator cuff tear arthropathy: pathophysiology, imaging characteristics, and treatment options. AJR Am J Roentgenol. 2015;205(5):W502–11. https://doi.org/10.2214/AJR.14.13815.
23. Ersoy H, Pomeranz SJ. Milwaukee shoulder syndrome. J Surg Orthop Adv. 2017;26(1):54–7.
24. Nguyen VD. Rapid destructive arthritis of the shoulder. Skeletal Radiol. 1996;25(2):107–12.
25. Husseini JS, Levin M, Chang CY. Capsular injury and inflammation. Magn Reson Imaging Clin N Am. 2020;28(2):257–67. https://doi.org/10.1016/j.mric.2019.12.008.

26. Mengiardi B, Pfirrmann CW, Gerber C, Hodler J, Zanetti M. Frozen shoulder: MR arthrographic findings. Radiology. 2004;233(2):486–92. https://doi.org/10.1148/radiol.2332031219.
27. Park S, Lee DH, Yoon SH, Lee HY, Kwack KS. Evaluation of adhesive capsulitis of the shoulder with fat-suppressed T2-weighted MRI: association between clinical features and MRI findings. AJR Am J Roentgenol. 2016;207(1):135–41. https://doi.org/10.2214/AJR.15.15200.
28. Messina C, Banfi G, Orlandi D, Lacelli F, Serafini G, Mauri G, Secchi F, Silvestri E, Sconfienza LM. Ultrasound-guided interventional procedures around the shoulder. Br J Radiol. 2016;89(1057):20150372. https://doi.org/10.1259/bjr.20150372.
29. Burke CJ, Rodrigues TC, Gyftopoulos S. Anterior instability: what to look for. Magn Reson Imaging Clin N Am. 2020;28(2):195–209. https://doi.org/10.1016/j.mric.2019.12.004.
30. Nacey NC, Fox MG, Bertozzi CJ, Pierce JL, Said N, Diduch DR. Incidence of gadolinium or fluid signal within surgically proven glenoid labral tears at MR arthrography. Skeletal Radiol. 2019;48(8):1185–91. https://doi.org/10.1007/s00256-018-3143-x.
31. Itoi E. 'On-track' and 'off-track' shoulder lesions. EFORT Open Rev. 2017;2(8):343–51. https://doi.org/10.1302/2058-5241.2.170007.
32. Albano D, Messina C, Sconfienza LM. Posterior shoulder instability: what to look for. Magn Reson Imaging Clin N Am. 2020;28(2):211–21. https://doi.org/10.1016/j.mric.2019.12.005.
33. Menashe SJ, Tse R, Nixon JN, Ishak GE, Thapa MM, McBroom JA, Iyer RS. Brachial plexus birth palsy: multimodality imaging of spine and shoulder abnormalities in children. AJR Am J Roentgenol. 2015;204(2):W199–206. https://doi.org/10.2214/AJR.14.12862.
34. Redondo-Alonso L, Chamorro-Moriana G, Jiménez-Rejano JJ, López-Tarrida P, Ridao-Fernández C. Relationship between chronic pathologies of the supraspinatus tendon and the long head of the biceps tendon: systematic review. BMC Musculoskelet Disord. 2014;15:377. https://doi.org/10.1186/1471-2474-15-377.
35. Schaeffeler C, Waldt S, Holzapfel K, Kirchhoff C, Jungmann PM, Wolf P, Stat D, Schröder M, Rummeny EJ, Imhoff AB, Woertler K. Lesions of the biceps pulley: diagnostic accuracy of MR arthrography of the shoulder and evaluation of previously described and new diagnostic signs. Radiology. 2012;264(2):504–13. https://doi.org/10.1148/radiol.12112007.
36. Buck FM, Dietrich TJ, Resnick D, Jost B, Pfirrmann CW. Long biceps tendon: normal position, shape, and orientation in its groove in neutral position and external and internal rotation. Radiology. 2011;261(3):872–81. https://doi.org/10.1148/radiol.11110914.
37. Petchprapa CN, Beltran LS, Jazrawi LM, Kwon YW, Babb JS, Recht MP. The rotator interval: a review of anatomy, function, and normal and abnormal MRI appearance. AJR Am J Roentgenol. 2010;195(3):567–76. https://doi.org/10.2214/AJR.10.4406.
38. Kassarjian A, Llopis E, Palmer WE. Distal clavicular osteolysis: MR evidence for subchondral fracture. Skeletal Radiol. 2007;36(1):17–22.
39. Sofka CM, Lin J, Feinberg J, Potter HG. Teres minor denervation on routine magnetic resonance imaging of the shoulder. Skeletal Radiol. 2004;33(9):514–8.
40. Williams MD, Edwards TB, Walch G. Understanding the importance of the teres minor for shoulder function: functional anatomy and pathology. J Am Acad Orthop Surg. 2018;26(5):150–61. https://doi.org/10.5435/JAAOS-D-15-00258.
41. Murphey MD, Flemming DJ, Boyea SR, Bojescul JA, Sweet DE, Temple HT. Enchondroma versus chondrosarcoma in the appendicular skeleton: differentiating features. Radiographics. 1998;18(5):1213–37; quiz 1244–1245